minerals

MDPI

Article

Bentonite Powder XRD Quantitative Analysis Using Rietveld Refinement: Revisiting and Updating Bulk Semiquantitative Mineralogical Compositions

Jaime Cuevas [1,*], Miguel Ángel Cabrera [1], Carlos Fernández [1], Carlos Mota-Heredia [1], Raúl Fernández [1], Elena Torres [2], María Jesús Turrero [2] and Ana Isabel Ruiz [1,*]

[1] Departamento de Geología y Geoquímica, Facultad de Ciencias, Universidad Autónoma de Madrid, 28049 Madrid, Spain; miguela.cabrera@estudiante.uam.es (M.Á.C.); carlos.fernandezramos@estudiante.uam.es (C.F.); carlos.mota@uam.es (C.M.-H.); raul.fernandez@uam.es (R.F.)

[2] CIEMAT, Av. Complutense 40, 28040 Madrid, Spain; elena.torres@ciemat.es (E.T.); mj.turrero@ciemat.es (M.J.T.)

* Correspondence: jaime.cuevas@uam.es (J.C.); anai.ruiz@uam.es (A.I.R.); Tel.: +34-914973047 (J.C.); +34-914976862 (A.I.R.)

Abstract: Bentonite is a claystone formed by a complex mineralogical mixture, composed of montmorillonite, illite, and accessory minerals like quartz, cristobalite, feldspars, carbonates, and minor amounts of iron oxy-hydroxides. Bentonite presents complexity at various scales: (1): a single mineral may present different chemical composition within the same quarry (e.g., feldspars solid solutions); (2): montmorillonite presents variability in the cation-exchange distribution while illite may be presented as mixed-layer with smectite sheets; and (3): hardness and crystal size are larger in accessory minerals than in clay minerals, preventing uniform grinding of bentonite. The FEBEX bentonite used is originally from Almería (Spain), and it is a predominantly calcium, magnesium, and sodium bentonite. This Spanish FEBEX bentonite has been hydrothermally altered at laboratory scale for 7–14 years. A thermal gradient was generated by heating a disk of pressed iron powder, simulating the metal waste canister, in contact with the compacted bentonite sample. Hydration was forced from the opposite direction. XRD recorded patterns were very similar. In order to minimize the bias of XRD semi-quantitative determination methods, Rietveld refinement was performed using BGMN software and different structural models. Confidence in the quantification of the main phases allows us to convincingly detect other subtle changes such as the presence of calcite in the hydration front, right at the interface between the saturated and unsaturated bentonite, or the presence of goethite, and not hematite, in the saturated bentonite, near the source of hydration. Smectite component was 72 ± 3% and the refinement was consistent with the presence of ~10% illite, comparable with previous characterizations.

Keywords: bentonite; montmorillonite; illite; Rietveld refinement; X-ray diffraction; iron-bentonite interaction

Citation: Cuevas, J.; Cabrera, M.Á.; Fernández, C.; Mota-Heredia, C.; Fernández, R.; Torres, E.; Turrero, M.J.; Ruiz, A.I. Bentonite Powder XRD Quantitative Analysis Using Rietveld Refinement: Revisiting and Updating Bulk Semiquantitative Mineralogical Compositions. *Minerals* **2022**, *12*, 772. https://doi.org/10.3390/min12060772

Academic Editor: Jordi Ibanez-Insa

Received: 25 April 2022
Accepted: 15 June 2022
Published: 17 June 2022

Publisher's Note: MDPI stays neutral with regard to jurisdictional claims in published maps and institutional affiliations.

1. Introduction

Bentonites are claystones, mainly formed by hydrothermal alteration of volcanic rocks [1–3]. They are mostly composed of clay minerals from the smectite family, a type of phyllosilicate that provides certain characteristics of interest as materials with structural functions of sealing, low permeability, and chemical barrier through cation-exchange processes.

Smectites are a group of clay minerals with a 2:1 phyllosilicate structure. The tetrahedral and octahedral sheets present isomorphic substitutions of mainly Si(IV) for Al(III)

and of Al(III) for Mg(II), respectively, so that an excess of negative charge is generated in the structure that constitutes a permanent layer charge. Its chemical formula can be expressed as $(M^{+}_{(x+y)}\cdot[(Al,Fe(III)_{(2-y)},Mg_y)\cdot Si_{(4-x)}Al_x\cdot O_{10}(OH)_2]\cdot nH_2O$. The presence of an interlayer space and the moderate magnitude of the laminar charge ($x + y < 0.6$) in its structure facilitate the entry of hydrated cations to neutralize the structural negative charge, and for this reason, smectite acts as a cation exchanger. Montmorillonites, as the most common smectites, present isomorphic substitutions in the inner sheet (octahedral), so the electrostatic force between the charged layers and the exchangeable cations in the interlayer zone is diffuse. This allows intercalation of cations coordinated with their sphere of solvating water molecules [4].

These structural characteristics explain at the molecular level one of the most important properties of montmorillonite: its swelling capacity in water. Besides, montmorillonite is a mineral with a very small crystal size, typically made up of laminar layer stacks of 10 nm in thickness × 50 nm in section [5], which facilitates its contact with an external solution. Bentonites have a wide variety of industrial uses: foundry molds for the steel industry, bentonite-drilling muds for use in excavation, binder for pellets, and as a construction material resistant to the passage of water, etc. [6]. However, one of its most prominent uses is chemical sealing and buffering, contemplated for the geological storage of high-level radioactive waste. In this context, not only the ability of bentonite to swell is important but also its very plastic behavior, ensuring that possible cracks formed by pressure in the host rock are easily sealed. In addition, compacted bentonite acquires very low hydraulic conductivity and has sufficient thermal conductivity to control pronounced temperature gradients. These characteristics cause the radionuclides transport mechanism to be predominantly diffusive and, therefore, have a very slow release to the geosphere. The high cation-exchange capacity is an important characteristic for retention of radionuclides in cationic form such as Cs, Sr, or Ni, abundant in burnt nuclear fuel, in the event of an accidental release [7,8]. Nowadays, the first high-level radioactive waste (HLRW) permanent repository is being constructed in Finland and an outer shell of compacted bentonite is planned to surround the copper canisters to be emplaced under license in 2024–2025 [9].

For this purpose, the bentonite barrier must be physically and chemically stable for thousands of years, so the bentonite used must, therefore, have a series of characteristics that ensure stability. The different accessory minerals it contains come into play in its chemical stability. According to ref. [10], who studied more than 10 high-grade bentonites thought to be used as compacted clay engineering barriers for HLRW confinement, the mineralogical composition of high grade bentonites is on average:

- 80 ± 10 wt.% smectite, mostly natural sodium exchanged forms. The sodium form has lower hydraulic conductivity and excellent swelling properties, in relation to other forms, such as calcium [11].
- <30 wt.% accessory minerals.

Accessory minerals may confer reactivity to bentonite and can interfere with its structural properties, leading to unwanted processes in the barrier. Calcite and pyrite can undergo acid-base and redox reactions. Gypsum is highly soluble, leading to the presence of porewater with high ionic concentrations, which also limit the swelling properties [12].

Consequently, it is very important to know the mineralogy of bentonite prior to the study of its applicability as a sealing material in an engineered barrier system. The most useful tool for the study of the mineralogical composition of predominantly crystalline materials is X-ray diffraction (XRD) of polycrystalline samples.

However, some mineralogical characteristics of bentonite have certain problems that can complicate their quantification study by XRD:

- A variable chemical composition, where isomorphic substitution is common, causes variation in X-ray diffraction patterns. In turn, the difference in cations located in the

interlayer space (mainly Mg^{2+}, Ca^{2+}, Na^{+}, and K^{+}) alter the positions of the characteristic reflections (e.g., [13,14]).

- Highly variable structures, which generate different types of interstratification and defects in three-dimensional space lattice, cause greater complexity in the X-ray diffraction patterns, compared with phases with a high degree of crystallinity [15].
- The preferential orientation of the smectite particles affects the signal intensities in pulverized samples. Phyllosilicates tend to be oriented in sheets, modifying the intensity of reflection compared to a random orientation and making analysis difficult. Preparation methods such as front loading tend to generate this preferential orientation [16].
- The mixture of different accessory minerals imposes other difficulties. The presence of small crystal size or amorphous silica polymorphs produce very broad signals in XRD that do not allow good quantification. On the other hand, potassium feldspars and plagioclases generate numerous reflections with very little reproducible intensities, due to the difference of grinding size and effects of preferred orientation when mixed with soft clay [17,18].

Quantification performed by X-ray diffraction can be grouped into single-reflection and full-pattern techniques. The former, including the RIR method, makes use of a specific reflection of the analyzed phase for its quantification of the weight percentage of the mineral sample, using the pure phase signal as a reference [16,19].

Despite their usefulness, individual reflection techniques present difficulties in determining multiphase samples that produce an overlapping of signals or present a certain preferential orientation. Clays are among these materials, due to their tendency to be oriented in a laminar way and their complex composition. Consequently, full pattern techniques have proven to be more effective in their analysis, especially the Rietveld method [20]. The Rietveld method [21] is a technique that theoretically adjusts the structural and experimental parameters to the complete powder diffractogram profile of the sample, considering it as the sum of the Bragg reflections that appear at respective angular positions, and using crystallographic data of each of the phases present in the material. It is a holistic approach to mineralogical quantification, rather than those techniques based on single reflections measurements.

Before performing a Rietveld refinement, it is necessary to define a series of functions that model the theoretical diffractogram, such as the signal profile function, full width at half maximum (FWHM), peak asymmetry, preferential orientation, and background, among others. Different software, such as SIROQUANT, TOPAS, or BGMN, was developed to define these functions through algorithms, and design theoretical structural models according to the Rietveld refining procedure [20].

This work aimed to carry out a reliable quantification of the minerals present in samples of FEBEX bentonite taken from a long-term experiment 14 years in duration, choosing the Rietveld method as the analysis technique. Previously used semiquantitative techniques in similar experiments [22] often produce uneven results in a series of determinations where apparently pattern differences are very small for slightly altered similar materials. With the use of this method, we discuss the consistency of differences produced by the alteration found in the characterization of a long-term reacted iron powder–bentonite interface.

2. Materials and Methods

2.1. Experiment

For the purpose of this research, Fe–bentonite cells (FB), designed and implemented by the CIEMAT (Centro de Investigaciones Energéticas, Medioambientales y Tecnológicas) in Madrid, Spain, have been used in long-term laboratory experiments of up to 14 years. A series of FB experiments were designed for the interpretation of the corrosion zone at the interface of a steel container (simulating a HLRW canister) and a compacted

bentonite (Spanish FEBEX reference), just as installed in the FEBEX in situ experiment [23]. Six cells (FB1 to FB6) were set up in August 2006 [24]. The bentonite cells are cylindrical with an internal diameter of 7 cm and an internal length of 10 cm. The FB cells were inserted into a Teflon cylinder to prevent lateral heat conduction. The top of the cells is made of a stainless steel cap. Inside this plug there is a water inlet, regulated at room temperature (25 °C) by recirculation from a water deposit. The bottom of the cells is a flat stainless steel heater at a temperature of 100 °C in contact with a 1.3 cm thick section of pressed iron powder. In this way, a constant temperature gradient is imposed between the top and bottom of the sample. The hydration of the bentonite was carried out through the top plug of the cell with water extracted from a pressurized stainless steel tank. A schematic diagram of the setup and a picture of the cells are shown in Figure 1. In this paper, the results of cell FB5, dismantled after 14 years of Fe-bentonite interaction, were used for XRD quantification as a function of the distance from the corroded iron powder hot zone. Water content of original bentonite dried in the laboratory environment was 14%. Hydration front in the experiment was localized in the transition of FB5_4 to FB5_3 sections (Figure 1).

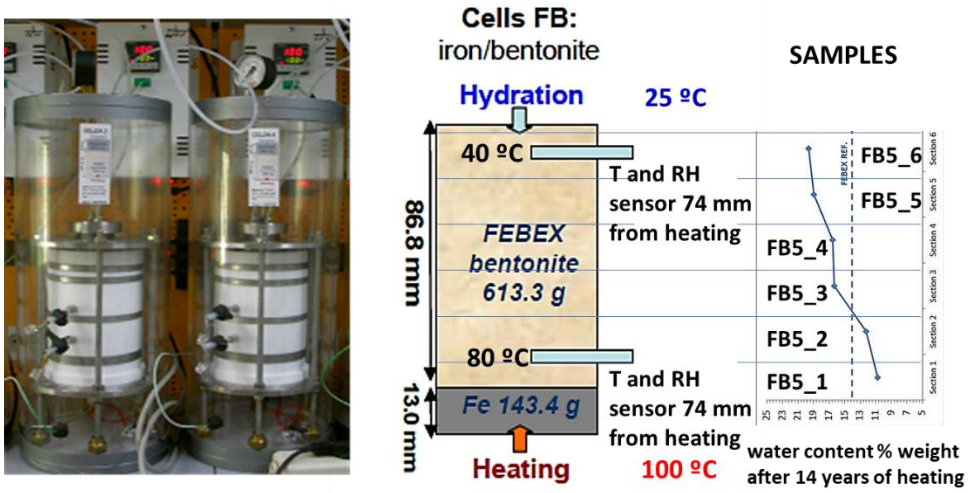

Figure 1. Image of the cells used to study the iron–bentonite interfaces. Diagram showing the configuration and location of the sensors in a FB cell and temperatures registered at the sensors before dismantling. Samples cut from the FB5 cell every 15 mm are numbered within the right graphic of water content evolution (5–25 weight % scale).

2.2. FEBEX Bentonite

FEBEX is a bentonite from Almería, Spain. It is a predominantly calcium, magnesium, and sodium (approximately 1/2, 1/4, 1/4 cation charge equivalents) bentonite. The montmorillonite in this bentonite has a small degree of intercalation of illite layers, so it is actually a randomly interstratified mixed layer illite/montmorillonite mineral, with 90 wt.% montmorillonite in its composition [25]. It also contains quartz, plagioclase, K-feldspar, calcite, and cristobalite [26,27]. Semi-quantification of this material has been presented in different reports, mostly based in the use of selected peak areas pondered by experimental correction factors as established by previous authors [28], RIR (reference intensity ratios) [16], or methods that include external calibrations using mixtures with common minerals as quartz [10]. Unfortunately, all these approaches seem to overestimate the clay minerals amount, as a representative mixture calibration, for instance, of silica polymorphs or feldspars is not possible to prepare. Moreover, critical difficulties are found to grind these hard minerals together with clay minerals, preventing their homogenization. Several data extracted from semi-quantified characterizations are compiled in Table 1. One trial was performed using the Rietveld refinement by means of the SIROQUANT© V3 software, from Sietronics Pty Limited. The results obtained in this first trial of Rietveld refinement were used to change some of the RIR data of minerals quantified (see notes in Table 1).

Then, the quantities, specifically for plagioclase mineral were increased significantly, both in refined or RIR quantified data (a) and (b) in Table 1. The scope of the present work is to check this quantification with another independent Rietveld refinement, including the potential to change structural models.

Table 1. Semi-quantification data for FEBEX bentonite mineralogy included in several reports.

Phase	[29]	[30]	[10]	(a)	(b)
Plagioclase	2 ± 1	1 ± 0.5	0.8 ± 0.2	5 ± 1	11.2
Cristobalite	2 ± 1	2 ± 0.5	1.6 ± 0.5	4.5 ± 1 (**)	1.2
Calcite	<1	1 ± 0.5	0.9 ± 0.2	0.8 ± 0.1 (**)	2.7
Goethite	-	-	-	+	-
Halite	-	-	-	-	-
Hematite	-	-	-	-	-
Maghemite	-	-	-	1	-
Magnetite	-	-	+	+	-
Illite	-	(10) *	1 ± 0.5	<1	-
Orthoclase	<1	2 ± 1	0.8 ± 0.2	+	-
Quartz	3 ± 1	2 ± 1	0.7 ± 0.2	4 ± 1	3.1
Smectite	>90	92 ± 3	94 ± 1	85 ± 2	81.5

*: % mixed layer Illite/Smectite using the method described by previous authors [31]. (a) Unpublished (RIR) method using the International Centre of Diffraction Data (ICDD) powder diffraction files (PDF) standards supported in High Score Expert Plus© software (version 2.1.b 2005). Some of the RIR were adjusted to fit a RIETVELD refinement quantification using SIROQUANT. (**) Calcite, Cristobalite, and Magnetite were quantified by acid degassing digestion and titration (calcite), alkaline dissolution (90 °C treatment of 0.05 g /25 mL NaOH 0.5 M and measurement of dissolved silica) (cristobalite) and by weighing magnetic fraction separated in a magnetic stirrer (magnetite). (b): Same as (a) Using SIROQUANT© software RIETVELD refinement without considering the aid of physical and chemical treatment for selected minerals quantification in (a). +: present; -: not detected. Note: References [10,29,30] are duplicate samples; (a) is an average of four different samples; (b) is the SIROQUANT© refinement of one FEBEX bentonite original sample.

Complementarily, to have another independent experimental measurement for the quantification of the major montmorillonite mineral, 5 g of bentonite by duplicate was weighed out and added to a 150 cm^3 centrifuge tube with distilled water. The tubes were placed in an ultrasonic bath to disperse the sample, and then centrifuged using a SIGMA™ swing-out rotor centrifuge. The necessary centrifuge time was calculated knowing the distance from the rotor axis to the bottom of the centrifuge tube, the height of the liquid in the tube, the average density of the particles (2.6 g/cm^3), and the size of the particles to be separated. These calculations were performed using the Centriset© software [29], obtaining that to sediment the fraction > 0.5 μm it was necessary to centrifuge for 5 min at 1500 rpm. After centrifugation, the supernatant was removed. The entire process of dispersion and sedimentation removing the suspension was repeated until the supernatant was transparent, which was the condition in which the separation was terminated. This >0.5 μm residue was weighed, considering the suspended rejected fraction as representative of clay fraction weight. This fraction was determined as 54.6 ± 2.5 wt.%. Small quantities of montmorillonite were detected in the residuals (fragments of altered volcanic rock were still present) and evaluated by the modified RIR method. Then, performing a correction for the residuals fraction, an amount of 78.6 ± 2.5 wt.% was determined to more accurately represent the clay fraction.

2.3. XRD Quantification

2.3.1. Use of BGMN© and the Profex Interface

BGMN (www.bgmn.de) was selected in this work due to the need to find a universal and precise model that could describe the shape of the signals within a wide range of °2θ angles [32]. Its design has capabilities that make it a potential tool for the analysis of multiphase materials such as clays, including optimization algorithm for the background calculation, a single step for calculation of the set of parameters of the initial model, correction of preferential orientations with anisotropic peak broadening, and the application of complex disorder models for implementation of real structural models. The profile function selected for the refinement was the pseudo-Voigt. Spherical harmonics were used as convolution factors to represent anisotropic crystal size and strain and asymmetric peak shape when using the lattice model. Research carried out with the software has successfully generated structural models of clay minerals for their quantitative analysis [33,34], as well as evaluating the degree of preferential orientation in them [35]. In addition, the free user interface Profex [36] facilitates the addition of subphases, consideration of amorphous phases in quantification results, or the conversion of crystallographic information from the CIF file into modifiable STR format for refining optimization.

For judging the quality of the Rietveld refinement fits, the most commonly used criteria are the discrepancy values (χ^2) and the agreement factors R (R_{wp}, R_{exp} and R_B). In general, smaller Rietveld error indices values indicate a better fit between the observed and calculated patterns. In particular cases, wrong models with poor-quality data may exhibit smaller values for error index than some good models with high-quality data. Therefore, they must never be used as the sole criterion for judging the quality of the profile fit. A graphical view of a fit is a necessary complement to evaluate the refinement quality. In this study, to evaluate the goodness-of-fit, χ^2 was the Rietveld discrepancy value considered. In addition, graphical examinations were performed for several examples and are shown in the paper.

2.3.2. XRD Equipment Parameters

The samples were measured in a Bruker D8 Discover diffractometer with Bragg–Brentano configuration, operating at a voltage of 40 kV and an intensity of 40 mA. It contains a primary monochromator, working with Cu Kα1 monochromatic radiation (λ = 1.54056 Å) and a fast multichannel LYNXEYE XE-T detector that discriminates fluorescence. The instrumental file to be considered in BGMN input parameters used was the "UIBK-D8-Discover-FDS-LynxEye", manually adding the wavelength used, and setting the minimum 2θ angle at 3 °2θ, and up to 65 °2θ, i.e., virtually the whole pattern registered. Samples were grinded by hand with an agate mortar and pestle until the fine powder was able to adhere to the walls. Adhered scales were grouped at the bottom and gently disaggregated with the pestle to form a fine powder. The powder was mounted by the backloading method in a 1.5 cm diameter circular holder.

The phases included in the refinement were all the minerals that were found both in previous characterizations of the bentonite and those identified in the first analysis of long-term FB experiments. Then, they were refined using structural models of quartz, albite, anorthite, orthoclase, calcite, cristobalite, muscovite1Md (illite), smectite_di2w, halite, goethite, and hematite. Maghemite and magnetite were also included but after refinement they were determined in <0.01 wt.%. In this paper, taking into account that the FEBEX montmorillonite interlayer was occupied mostly by divalent cations in the smectite interlayer, and that samples were dried at ambient conditions, the di-hydrated structure of dioctahedral smectite was used. In order to maintain divalent cation di-hydrated environmental conditions, samples were equilibrated with a 50% relative humidity using a $MgNO_3$-saturated solution environment.

3. Results

3.1. FEBEX Bentonite

The original bentonite XRD pattern was first refined. The refinement, in a first step, included a selection of an appropriate structural model for the smectite phase. An initial search into the Crystallography Open Database (COD) CIF files showed a match for a montmorillonite structural model [37]. After inspection of the obtained refinement, the theoretical diffractogram did not align well with the experimental pattern. Therefore, such model was discarded in favor of a more general structural model of a turbostratic disordered di-hydrated smectite [33], resulting in a better match at °2θ angles of 6.0° (001), 19.7° (020, 110), 34.7° (040, 220), 54.0° (150, 240, 310), and 61.6° (060, 330).

Most of the sharp narrow peaks in the 26–32 °2θ were identified as plagioclase. Then, structural models of plagioclase were searched for a better refinement in the range of °2θ angles 26–32°. The patterns of plagioclase in this range may vary significantly within different diffractograms of several FEBEX bentonite samples. An initial approach was to use Anorthite and Albite from the BGMN database for an estimated composition, followed by a refinement using composition of Albite:Anorthite 40:60 Labradorite. Due to plagioclase isomorphism, the refinement was not as successful as expected, but suggested the idea of using subphases of Albite and Anorthite to consider their compositional variability within the bentonite. This resulted in the better fit and refinement if, in addition, the structural models of their high-crystallinity phases were used [38,39]. Figure 2 shows the differences in pattern refinement for the selected region of 21.0–31.0 °2θ, using the BGMN database compared with the use of the mentioned high-crystallinity structural models.

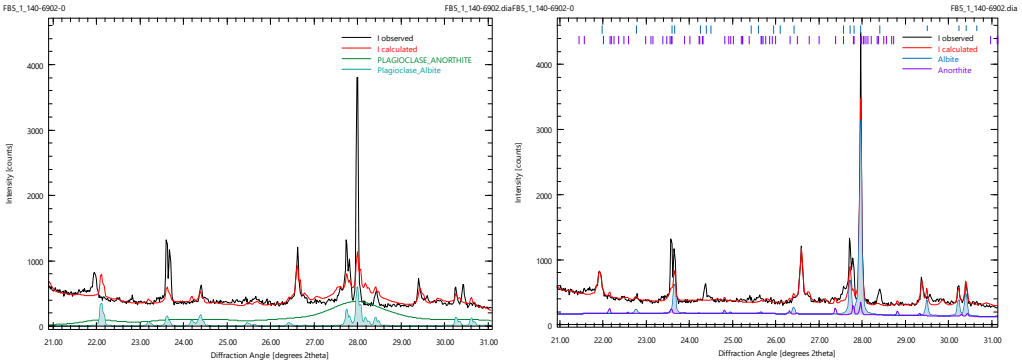

Figure 2. Patterns showing the refinement of bentonite in the region of plagioclase main reflections in the range of 21.0–31.0 °2θ. Pattern in the right side show the better refinement by using the structural models proposed by previous authors [38,39].

The (hk0) reflections attributed to montmorillonite, for instance 34.7 °2θ, cannot be completely resolved in the theoretical pattern, as the shape of the band is not properly refined in most diffractograms. Illite (disordered 1Md muscovite phase) addition in the refinement led to a substantially better theoretical pattern fit and a better resolution for the referred reflection and, in general (hk0) indexed peaks. Figure 3 shows the impact in the refinement with and without Illite addition.

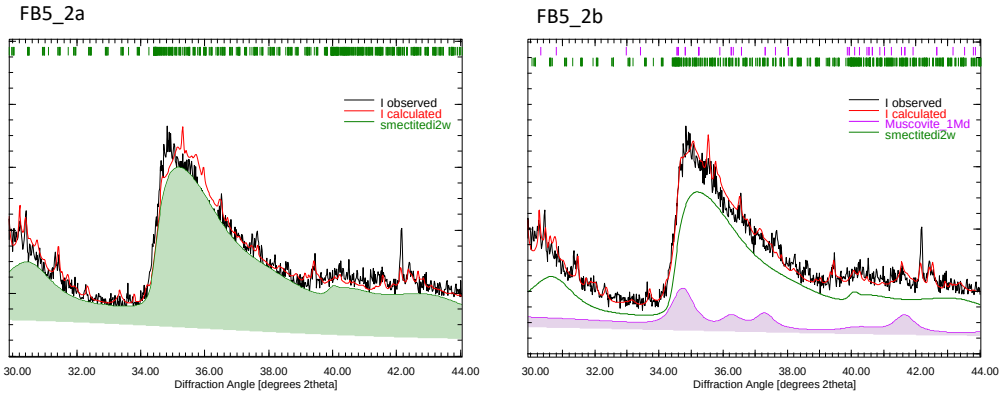

Figure 3. BGMN Rietveld refinement example of the region at 34.7 °2θ showing the (040) and (220) reflections attributed to montmorillonite. Effect of the addition of the Muscovite_1Md structural model to smectitedi-2w (right side).

The complete group of identified minerals was added to the refinement without further modifications of the corresponding STR files in BGMN, as some trials of changes of their parameters resulted in no significant change of their theoretical diffractograms. After quantification, mineralogical phases with a composition < 0.01% were discarded from subsequent refinements, further improving the theoretical diffractograms. Figure 4 shows the aspect of the refinement for a sample of the complete FEBEX original bentonite.

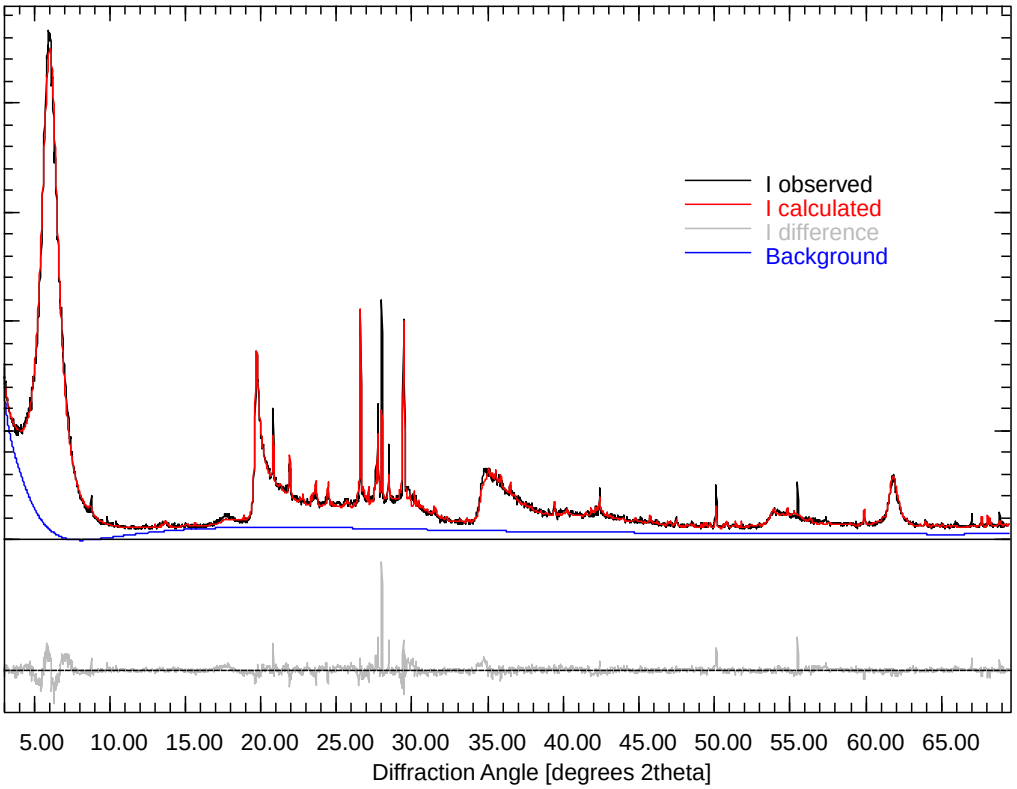

Figure 4. BGMN refinement of a sample of original FEBEX bentonite. Mineral quantification and goodness of fit are shown in Table 2.

Table 2 shows quantification after the refinement of the original bentonite and the bentonites refined after the 14 years experiment determined in the six sections analyzed, cut and separated approximately every 1.5 cm (Figure 1).

Table 2. Quantification (wt.%) after BGMN© refinement ($\chi^2 < 5$).

Phase	FEBEX	FB5_1	FB5_2	FB5_3	FB5_4	FB5_5	FB5_6
Plagioclase	7.7	11.8	14.8	9.5	13.0	9.7	16.5
Cristobalite	-	0.5	0.3	0.3	0.3	0.3	0.4
Calcite	0.9	0.6	1.8	0.6	3.9	1.1	2.2
Goethite	0.5	-	0.6	0.5	1.4	2.2	-
Halite	-	-	0.1	0.1	0.1	0.1	-
Hematite	-	-	-	-	-	-	-
Maghemite	-	-	-	0.1	-	0.2	-
Magnetite	0.4	-	-	-	-	0.1	-
Illite	12.7	1.3	9.5	11.9	11.0	8.1	7.1
Orthoclase	2.4	2.5	1.8	1.8	1.8	1.3	2.55
Quartz	2.5	3	1.1	2.5	1.0	1.0	1.5
Smectite	73.0	82.0	70.0	72.6	67.5	75.9	69.2
χ^2	2.93	3.6	3.6	2.6	2.9	2.5	4.8

3.2. FB 5 Hydrothermal Experiment

Figure 5 show the result of FB5 bentonite experiments samples refinement in three sections of interest, FB5_1, FB5_3, and FB5_5, respectively, going from the heating to the hydration end. Despite evident variations in the presence of sharp thin reflections, the refinement of the whole pattern determines mineral weight % that are relatively homogeneous comparing these series of similar FEBEX bentonite samples with a good agreement quality validated by $\chi^2 < 5$ statistical parameters.

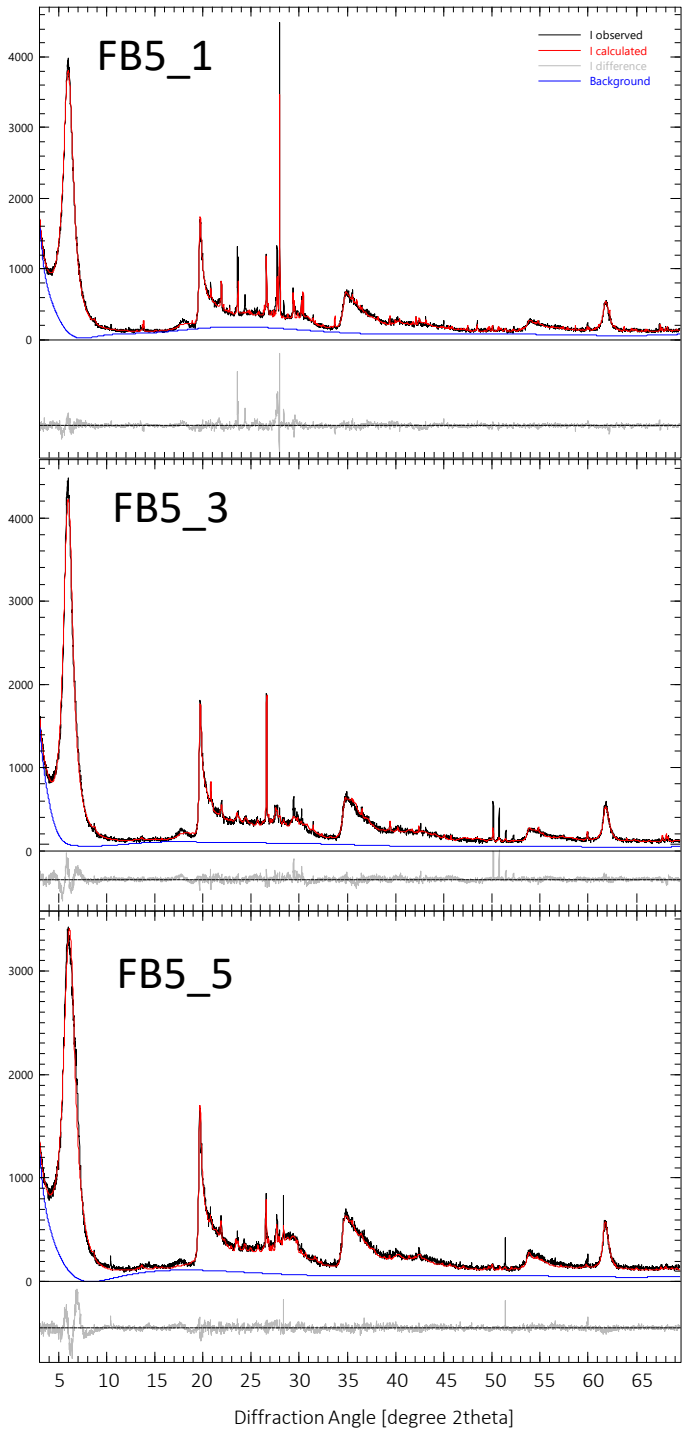

Figure 5. FB5 experiment samples refinement in three sections of interest, FB5_1, FB5_3, and FB5_5, respectively, going from the heating to the hydration zone of the FB iron–bentonite hydrothermal experiment.

Several aspects of the quantification of this series of samples can be discussed subsequently to be consistent with expected general effects presented on bentonite mineralogy.

4. Discussion of Results

The experiments carried out are characterized by the existence of two opposite hydrothermal gradients affecting a bentonite barrier. A groundwater hydration front is to be developed against the heat (approximately 100 °C in the metal waster canister surface) that will be produced by the active disintegration of burnt fuel radioisotopes during the

first 100 years in an active high-level nuclear waste repository [40]. As a consequence, reactive processes characteristic of hydrothermal alteration should be expected to be observed in the analyzed long-term experiments.

The results obtained by mineralogical quantification using the BGMN software and the optimized selection of certain structural models produced a set of comparable and homogeneous results in which some processes expected in long-term hydration and heating experiments were observed.

Relatively long-term laboratory experiments (up to 5–15 years) have been conducted under repository conditions in which FEBEX bentonite has experimented minor alteration (e.g., [41,42]), with qualitative evidence on impacts on mineralogical and geochemical properties. These authors have reported a minor dissolution of smectite and a limited increase in the formation of mixed-layer illite–smectite. This irreversible dehydration process (illite or collapsed smectite structure production) and the loss of the expansive swelling component (smectite) are very important variables to be quantified in the experiments. Swelling under hydration (swelling pressure) and cation-exchange properties are the key for hydromechanical isolation and chemical buffering functions of bentonite clay rock [43].

Our quantification results are in agreement with the abovementioned minor alteration of the bentonite claystone as a whole. Considering the samples to be very similar to the original bentonite, Illite composition yielded a weight % near 10%, very similar to that determined by previous authors [25] in FEBEX bentonite by means of analysis of regularity of basal reflections (interlayer periodicity) using specific XRD-oriented preparation. It is known that other XRD-specific tests are necessary to be performed (e.g., [44]) to qualitatively ascertain of the nature of the mixed layering, often complemented with chemical analysis of the clay fraction. Then, the BGMN refinement was able to include the mixture of illite with montmorillonite in the quantification, which was not possible in the routine procedures for semi-quantification of FEBEX bentonite. Moreover, the sum of smectite and illite is very close to the 80% weight determined by the gravimetric analysis described in the methodology for the clay minerals fraction.

XRD powder pattern of the iron interface FB5_1 sample can be refined without considering the illite component, maintaining the 80% weight for smectite accounting for the clay minerals content. This effect may be an anomaly or a structural change that has to be elucidated. The progression of illite to smectite has been reported under <100 °C temperatures in similar hydrothermal alteration of bentonites [45].

Other mineralogical changes related to dissolution and precipitation processes are also important to check. Soluble ions transported from cold hydrated zones to warm dehydrated zones can lead to precipitation of halite, anhydrite, gypsum, or calcite in hydrated to dehydrated transition zones. Dehydration heat zones are water evaporative environments in which solutions become more concentrated [41]. In these critical zones, and in connection to alkaline environments (concrete, iron oxidation), the formation of silica minerals has also been reported [46].

In terms of potential precipitation processes, calcite proportion in sample was increased up to approximately 4% near the limit in which the hydration front (water saturated bentonite) was stopped by the heat gradient (sample FB5_4). The precipitation of sparingly soluble components in this evaporative interface is, therefore, highly probable as has been argued before [41]. It is worth to mention that in the bentonite water-saturated zone FB5_5, goethite iron oxyhydroxide was present while it was absent close to the hot iron powder zone (FB5_1). Again, this is very consistent with the hydrated environmental conditions of the experiment. Conversely, in the section in contact with the hydration source (FB5_6), no iron oxyhydroxides were detected and the maximum goethite was in FB5_5. Then, it is necessary to check the possibility of goethite dissolution and precipitation of iron oxy-hydroxide with the advance of the hydration front (in FB5_5). Precipitation of goethite, at moderate temperatures > 50 °C in alkaline pH, by transformation of Fe (III)-precipitated hydroxide is documented in the literature [47].

Cristobalite was not quantified in the BGMN refinement of the original FEBEX bentonite and was present in all samples with a maximum relative value found for FB5_1. There is no evidence for significant dissolution–precipitation processes of silica in the bulk samples analyzed in this experiment compared to observations in alkaline interfaces of FEBEX bentonite [46].

Finally, it is worth mention that differences between theoretical and experimental diffractograms for the di-hydrated montmorillonite peak at 6.0 °2θ increased as the analyzed section became closer to the hydration end (Figure 6). This suggest the formation of a secondary phase of sodium montmorillonite by ion exchange substitution, being a process more favorable for regions in contact with water containing ions in solution rather than in relatively drier regions close to the heating end. Many long-term hydration experiments, under an imposed heat gradient, behave in the sense of concentrated Na and Ca in the exchangeable cation smectite complex near the hydration source and conversely Mg and less Ca with minor Na near the warmer dry zones [48].

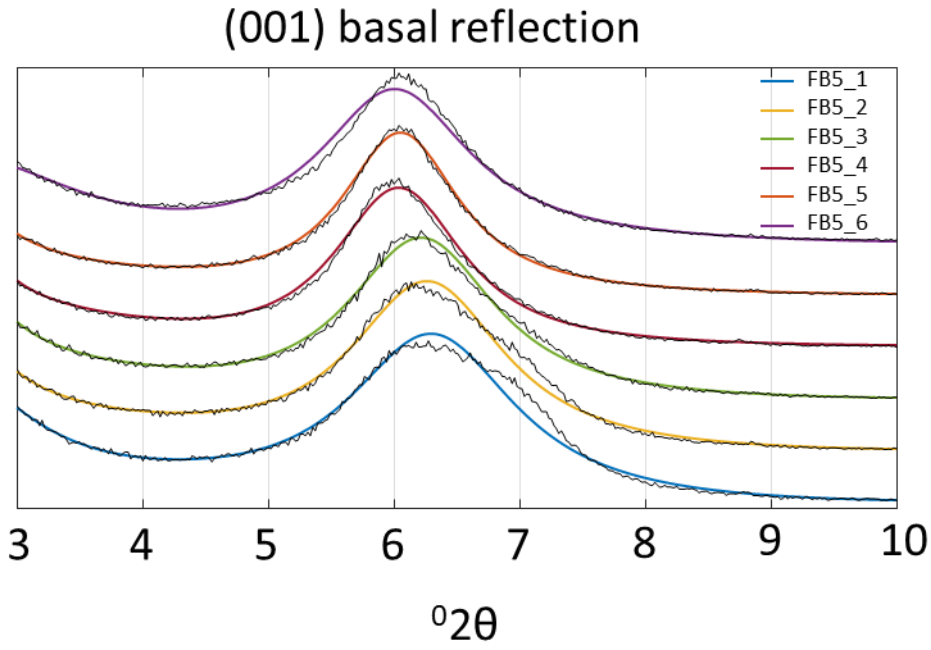

Figure 6. Angular position of (001) basal reflection. Displacement and experimental curves broadening at high angular positions for FB5_3 to FB5_5 (see text).

5. Conclusions

Summarizing the quantification results, they were in reasonable agreement with the type of alteration that was expected in the bentonite analyzed. More important is that clay mineral percentages were in close agreement with the experimental weighting method used as a complementary test and using two different Rietveld approaches, SIROQUANT© and BGMN. The whole pattern refinement reduces the high uncertainty developed in using height or areas to measure the intensity of mayor peaks. Nevertheless, is important to check structural models that adequately yield an optimum fitting to mineral phases involved, in particular those affected by being representative of complex solid solutions as feldspars or to intervene in the formation of mixed layering as illite.

Further work is also needed to follow in gaining confidence and improving the quality of quantification of accessory minerals. It is needed also to implement the refinement of the proportion of 1w and 2w hydrates in the montmorillonite present in the bentonite by means of considering an adequate structural model.

Author Contributions: Conceptualization, J.C., M.Á.C., C.F. and A.I.R.; Data curation, J.C. and A.I.R.; Formal analysis, J.C., M.Á.C., C.F. and A.I.R.; Funding acquisition, J.C., M.J.T. and A.I.R.; Investigation, J.C., C.F., C.M.-H., R.F., E.T., M.J.T. and A.I.R.; Methodology, J.C., M.Á.C., C.F. and A.I.R.; Project administration, J.C. and A.I.R.; Resources, J.C., M.Á.C., C.F., C.M.-H., R.F., E.T., M.J.T. and A.I.R.; Software, J.C., M.Á.C., C.F. and A.I.R.; Supervision, J.C. and A.I.R.; Validation, J.C., M.J.T. and A.I.R.; Visualization, J.C., M. Á.C., C.F., C.M.-H., R.F., E.T., M.J.T. and A.I.R.; Writing – original draft, J.C.; Writing—review & editing, A.I.R. All authors have read and agreed to the published version of the manuscript.

Funding: The research presented in this manuscript belongs to the EURAD-ACED Project which has received funding from the European Union's Horizon 2020 research and innovation programme under grant agreement No 847593.

Conflicts of Interest: The authors declare no conflict of interest.

References

1. Caballero, E.; de Cisneros, C.J.; Huertas, F.J.; Pozzuoli, A.; Linares, J. Bentonites from Cabo de Gata, Almería, Spain: A mineralogical and geochemical overview. *Clay Miner.* **2005**, *40*, 463–480. https://doi.org/10.1180/0009855054040184.
2. Christidis, G.; Huff, W.D. Geological Aspects and Genesis of Bentonites. *Elements* **2009**, *5*, 93–98. https://doi.org/10.2113/gselements.5.2.93.
3. Gilg, H.A.; Kaufhold, S.; Ufer, K. Smectite and Bentonite Terminology, Classification, and Genesis. In *Bentonites. Characterization, Geology, Mineralogy, Analysis, Mining, Processing and Uses*; Kaufhold, S., Ed.; Publisher Geologisches Jahrbuch Reihe B: Hannover, Germany; 2002; pp. 1–18, 400, Band B 106. https://doi.org/10.1127/bentonites/9783510968596.
4. Güven, N. Molecular Aspects of Clay-Water Interactions. In *Clay-Water Interface and Its Rheological Implications (CMS Workshop lectures, vol 4)*; Güven, N.; Pollastro, R.M., Eds.; The Clay Minerals Society: Boulder, CO, USA, 1992.
5. Żbik, M.S.; Martens, W.; Frost, R.L.; Song, Y.-F.; Chen, Y.-M.; Chen, J.-H. Transmission X-ray Microscopy (TXM) Reveals the Nanostructure of a Smectite Gel. *Langmuir* **2008**, *24*, 8954–8958. https://doi.org/10.1021/la800986t.
6. Odom, I.E. Smectite clay minerals: Properties and uses. *Philos. Trans. R. Soc. Lond. Ser. A Math. Phys. Sci.* **1984**, *311*, 391–409. https://doi.org/10.1098/rsta.1984.0036.
7. Weber, W.; Navrotsky, A.; Stefanovsky, S.; Vance, E.R.; Vernaz, E. Materials Science of High-Level Nuclear Waste Immobilization. *MRS Bull.* **2009**, *34*, 46–53. https://doi.org/10.1557/mrs2009.12.
8. Cohen, B.L. High-level radioactive waste from light-water reactors. *Rev. Mod. Phys.* **1977**, *49*, 1–20. https://doi.org/10.1103/RevModPhys.49.1.
9. El-Showk, S. Final resting place. *Science* **2022**, *375*, 806–810. https://doi.org/10.1126/science.ada1392.
10. Cuevas, J.; Fernández, R.; Ortega, A.; Ruiz, A.I. *Comparison of Alternative Bentonites for Potential Use as Buffer and Sealing Materials in the Swiss Concept for Ra-Dioactive Waste Disposal. Part 2: Results*. Nagra Arbeitsbericht Wettingen, Switzerland NAB: 2014; pp. 14–65.
11. Gates, W.P.; Bouazza, A.; Churchman, G.J. Bentonite Clay Keeps Pollutants at Bay. *Elements* **2009**, *5*, 105–110. https://doi.org/10.2113/gselements.5.2.105.
12. Madsen, F.T.; Müller-Vonmoos, M. The swelling behaviour of clays. *Appl. Clay Sci.* **1989**, *4*, 143–156. https://doi.org/10.1016/0169-1317(89)90005-7.
13. Bergaya, F.; Lagaly, G. General Introduction: Clays, Clay Minerals, and Clay Science. In *Handbook of Clay Science: Developments in Clay Science, Vol. 1*; Bergaya, F., Theng, B.K.G., Lagaly, G., Eds.; Elsevier: The Netherlands, Amsterdam, 2006. https://doi.org/10.1016/S1572-435201001-9.
14. Liu, D.; Yuan, P.; Liu, H.; Cai, J.; Tan, D.; He, H.; Zhu, J.; Chen, T. Quantitative characterization of the solid acidity of montmorillonite using combined FTIR and TPD based on the NH3 adsorption system. *Appl. Clay Sci.* **2013**, *80*, 407–412. https://doi.org/10.1016/j.clay.2013.07.006.
15. Srodon, J. Quantitative mineralogy of sedimentary rocks with emphasis on clays and with applications to K-Ar dating. *Miner. Mag.* **2002**, *66*, 677–687. https://doi.org/10.1180/0026461026650055.
16. Hillier, S. Accurate quantitative analysis of clay and other minerals in sandstones by XRD: Comparison of a Rietveld and a reference intensity ratio (RIR) method and the importance of sample preparation. *Clay Miner.* **2000**, *35*, 291–302. https://doi.org/10.1180/000985500546666.
17. Bish, D.L.; Reynolds, R.C. Jr. Sample preparation for X-ray Diffraction. In *Reviews in Mineralogy, Vol. 20, Modern Powder Diffraction*; Bish, D.L., Post, J.E., Eds.; The Mineralogical Society of America: Washington, WA, USA, 1989.
18. Ali, A.; Chiang, Y.W.; Santos, R.M. X-ray Diffraction Techniques for Mineral Characterization: A Review for Engineers of the Fundamentals, Applications, and Research Directions. *Minerals* **2022**, *12*, 205. https://doi.org/10.3390/min12020205.
19. Chung, F.H. Quantitative interpretation of X-ray diffraction patterns of mixtures. II. Adiabatic principle of X-ray diffraction analysis of mixtures. *J. Appl. Crystallogr.* **1974**, *7*, 519–525. https://doi.org/10.1107/S0021889874010375.

20. Zhou, X.; Liu, D.; Bu, H.; Deng, L.; Liu, H.; Yuan, P.; Du, P.; Song, H. XRD-based quantitative analysis of clay minerals using reference intensity ratios, mineral intensity factors, Rietveld, and full pattern summation methods: A critical review. *Solid Earth Sci.* **2018**, *3*, 16–29. https://doi.org/10.1016/j.sesci.2017.12.002.
21. Rietveld, H.M. A profile refinement method for nuclear and magnetic structures. *J. Appl. Crystallogr.* **1969**, *2*, 65–71. https://doi.org/10.1107/s0021889869006558.
22. Fernández, R.; Torres, E.; Ruiz, A.I.; Cuevas, J.; Alonso, M.C.; Calvo, J.L.G.; Rodríguez, E.; Turrero, M.J. Interaction processes at the concrete-bentonite interface after 13 years of FEBEX-Plug operation. Part II: Bentonite contact. *Phys. Chem. Earth Parts A/B/C* **2017**, *99*, 49–63. https://doi.org/10.1016/j.pce.2017.01.009.
23. Torres, E.; Escribano, A.; Baldonedo, J.L.; Turrero, M.J.; Martin, P.L.; Peña, J.; Villar, M.V. Evolution of the Geochemical Conditions in the Bentonite Barrier and Its Influence on the Corrosion of the Carbon Steel Canister. In Proceedings of the Materials Research Society Symposium Fall Meeting, Boston, MA, USA, 1-5 December 2008.
24. Torres, E. *Geochemical Processes at the C-Steel / Bentonite Interface in a Deep Geological Repository: Experimental Approach and Modeling*. Unpublished PhD. Universidad Complutense de Madrid, Madrid, Spain, 2011.
25. Cuadros, J.; Linares, J. Experimental kinetic study of the smectite-to-illite transformation. *Geochim. et Cosmochim. Acta* **1996**, *60*, 439–453. https://doi.org/10.1016/0016-7037(95)00407-6.
26. Huertas, F.; Fariñas, P.; Farias, J.; García-Siñeriz, J.L.; Villar, M.V.; Fernández, A.M.; Martín, P.L.; Elorza, F.J.; Gens, A.; Sánchez, M.; et al. *Full-Scale Engineered Barriers Experiment. Updated Final Report 1994–2004*; Enresa Technical Report 05-0/2006; Madrid, Spain, 2006.
27. Villar, M.; Fernández, A.; Rivas, P.; Lloret, A.; Daucausse, D.; Montarges-Pelletier, E.; Devineau, K.; Villieras, F.; Hynkova, E.; Cechova, Z.; et al. (eds.); *FEBEX Project Final Report. Post-Mortem Bentonite Analysis*; Enresa Technical Report 05-1/2006; Madrid, Spain, 2006.
28. Martín Pozas, I.M.; Martín Vivaldi, J.L.; Rodríguez Gallego, M. Análisis cuantitativo de filosilicatos de la arcilla por difracción de rayos X. *An. Real Soc. Esp. Fis. Y Quim. Serie B* **1969**, *55*, 109–112.
29. Poppe, L.J.; Eliason, A.E. A basic program to calculate gravitational and centrifugal settling parameters. *Geol. Soc. Am.* **2009**, *41*, 21.
30. Ramírez, S. Hydrothermal Alteration of "La Serrata" Bentonite (Almería, Spain) by Alkaline Solutions. Ph.D. Thesis Universidad Autónoma de Madrid, Madrid, Spain, 2002.
31. Inoue, A.; Bouchet, A.; Velde, B.; Meunier, A. Convenient technique for estimating smectite layer percentage in randomly interstratified illite/smectite minerals. *Clays Clay Miner.* **1989**, *37*, 227–234. https://doi.org/10.1346/CCMN.1989.0370305.
32. Bergmann, J.; Kleeberg, R.; Taut, T.; Haase, A. Quantitative Phase Analysis Using a New Rietveld Algorithm—Assisted by Improved Stability and Convergence Behavior. In Proceedings of the 45th annual X-Ray conference in Denver, Colorado, 3-8 August 1996. Advances in X-Ray Analysis, 40 (1998), 425 (published on CD-ROM).
33. Ufer, K.; Roth, G.; Kleeberg, R.; Stanjek, H.; Dohrmann, R.; Bergmann, J. Description of X-ray powder pattern of turbostratically disordered layer structures with a Rietveld compatible approach. *Z. Für Krist. -Cryst. Mater.* **2004**, *219*, 519–527. https://doi.org/10.1524/zkri.219.9.519.44039.
34. Ufer, K.; Stanjek, H.; Roth, G.; Dohrmann, R.; Kleeberg, R.; Kaufhold, S. Quantitative phase analysis of bentonites by the Rietveld method. *Clays Clay Miner.* **2008**, *56*, 272–282. https://doi.org/10.1346/CCMN.2008.0560210.
35. Kleeberg, R.; Monecke, T.; Hillier, S. Preferred orientation of mineral grains in sample mounts for quantitative XRD measurements: How random are powder samples? *Clays Clay Miner.* **2008**, *56*, 404–415. https://doi.org/10.1346/CCMN.2008.0560402.
36. Doebelin, N.; Kleeberg, R. Profex: A graphical user interface for the Rietveld refinement program BGMN. *J. Appl. Crystallogr.* **2015**, *48*, 1573–1580. https://doi.org/10.1107/S1600576715014685.
37. Viani, A.; Gualtieri, A.F.; Artioli, G. The nature of disorder in montmorillonite by simulation of X-ray powder patterns. *Am. Mineral.* **2002,** *87*, 966–975. https://doi.org/10.2138/am-2002-0720.
38. Prewitt, C.T.; Sueno, S.; Papike, J.J. The crystal structures of high albite and monalbite at high temperatures. *Am. Mineral.* **1976**, *61*, 1213–1225.
39. Wainwright, J.E.; Starkey, J. A refinement of the structure of anorthite. *Zeitschrift für Kristallographie-Crystalline Materials* **1971**, *133*, 75–84. https://doi.org/10.1524/zkri.1971.133.16.75.
40. Zhou, X.; Zhou, A.; Sun, D. Three-dimensional thermal analysis of the repository for high-level radioactive nuclear waste. *Int. J. Energy Res*. **2020,** *44*, 8208– 8220. https://doi.org/10.1002/er.5400.
41. Gómez-Espina, R.; Villar, M.V. Effects of heat and humidity gradients on MX-80 bentonite geochemistry and mineralogy. *Appl. Clay Sci.* **2015**, *109*, 39–48. https://doi.org/10.1016/j.clay.2015.03.012.
42. Villar, M.V.; Martín, P.L.; Bárcena, I.; García-Siñeriz, J.L.; Gómez-Espina, R.; Lloret, A. Long-term experimental evidences of saturation of compacted bentonite under repository conditions. *Eng. Geol.* **2012**, *149*, 57–69. https://doi.org/10.1016/J.ENGGEO.2012.08.004.
43. Sellin, P.; Leupin, O.X. The use of clay as an engineered barrier in radioactive-waste management a Review. *Clays Clay Miner.* **2013**, *61*, 477–498. https://doi.org/10.1346/CCMN.2013.0610601.
44. Plançon, A. Consistent Modeling of the XRD Patterns of Mixed-layer Phyllosilicates. *Clays Clay Miner.* **2004**, *52*, 47–54. https://doi.org/10.1346/CCMN.2004.0520106.

45. Xie, M.; Miehe, R.; Kasbohm, J.; Herbert, H.-J.; Meyer, K.; Ziesche, U. Bentonite Barriers –New Experiments and State of the Art. Bentonite as Barrier Material for the Sealing of Underground Disposal Sites. Final Report. GRS–300: 2012. ISBN 978-3-939355-79-3.
46. Turrero, M.J.; Villar, M.V.; Torres, E.; Escribano, A.; Cuevas, J.; Fernández, R.; Ruiz, A.I.; Vigil de la Villa, R.; de Soto, I. Long-term Performance of Engineered Barrier Systems PEBS Contract (grant agreement) number: FP7 249681, DELIVERABLE (D-N°:D2.3-3-1). Laboratory tests at the interfaces (First results on the dismantling of tests FB3 and HB4), 31/10/2011.
47. Das, S.; Hendry, M.J.; Essilfie-Dughan, J. Transformation of two-line ferrihydrite to goethite and hematite as a function of pH and temperature. *Environ. Sci. Technol.* **2011**, *45*, 268–275. https://doi.org/10.1021/es101903y.
48. Villar, M.V. *FEBEX-DP Post-mortem. THM/THG Analysis Report*. Arbeitsbericht NAB 2017; pp. 16–17.